Earth Planets Space, **59**, 401–405, 2007

Variations in the equatorial ionization anomaly peaks in the Western Pacific region during the geomagnetic storms of April 6 and July 15, 2000

Chien-Hung Lin[1], Jann-Yenq Liu[2,3], Ho-Fang Tsai[4], and Chio-Zong Cheng[1,5]

[1]*National Space Organization, Hsinchu, Taiwan*
[2]*Institute of Space Science, National Central University, Chung-Li, Taiwan*
[3]*Center for Space and Remote Sensing Research, National Central University, Chung-Li, Taiwan*
[4]*Central Weather Bureau, Taipei, Taiwan*
[5]*Plasma and Space Science Center, National Cheng-Kung University, Tainan, Taiwan*

(Received September 5, 2006; Revised February 13, 2007; Accepted February 15, 2007; Online published June 8, 2007)

This study utilizes total electron content (TEC) observed by a network of ground-based GPS receivers located in the Western Pacific region (∼120°E) to study the responses of the low-latitude equatorial ionization anomaly (EIA) to the two major magnetic storms that occurred during April 4–10 and July 12–18, 2000. The latitude, time, and TEC (LTT) maps in the northern and southern EIA regions show that both EIA peaks move equatorward along with a pronounced reduction of the TEC values 10–12 h after the storm onset. The variations in the EIA peak TEC values and locations in the northern EIA are highly correlated with those in the southern EIA. The correlation coefficients of the day-to-day variations of peaked TEC between the northern and southern EIA regions are 0.75 in the April storm and 0.83 in the July storm. The correlation coefficients of the day-to-day EIA peak movements between the two hemispheres are 0.98 in the April storm event and 0.88 in the July storm event. The highly correlated peaked TEC and movements between the northern and the southern hemisphere suggest that the storm-produced electrodynamics played a dominant role in affecting the low-latitude ionosphere during the two major storms.

Key words: Low-latitude equatorial ionization anomaly, Western Pacific region, Magnetic storms, Total electron content.

1. Introduction

During magnetic storms, the ionospheric electric field, neutral wind, and neutral composition have often been observed to deviate from their quiet time patterns (e.g. Fesen *et al*., 1989; Fejer and Scherliess, 1995; Prölss, 1995; Fuller-Rowell *et al*., 1997; Buonsanto, 1999; Kil *et al*., 2003; Lin *et al*., 2005a). These storm-generated disturbances in electric field, neutral wind, and neutral composition significantly affect the low-latitude ionosphere. The low-latitude ionosphere is characterized by the equatorial ionization anomaly (EIA) produced by the equatorial plasma fountain (Namba and Maeda, 1939; Appleton, 1946; Duncan, 1960; Hanson and Moffett, 1966; Anderson, 1973; Balan and Bailey, 1995; Rishbeth, 2000). The equatorial plasma fountain is produced by a daytime eastward electric field that produces an upward $\mathbf{E}\times\mathbf{B}$ drift which lifts the plasma to higher altitudes, from where it diffuses down along magnetic field lines to higher latitudes to create two ionization crests on both sides of the magnetic equator. Therefore, the strength and polarity of the zonal electric field would affect the equatorial plasma fountain and EIA morphology. During magnetic storms, the storm-generated zonal electric fields may enhance or reduce the daytime eastward electric field and thus result in a stronger or a weaker plasma fountain, respectively. In general, the storm-generated electric fields can be identified as a short-lived prompt penetration electric field originating from the solar wind-magnetospheric dynamo (e.g. Jaggi and Wolf, 1973; Kelley *et al*., 1979; Senior and Blanc, 1984; Spiro *et al*., 1988; Kelley *et al*., 2003; Maruyama *et al*., 2005) and a longer time-lasting disturbance dynamo electric field (e.g. Blanc and Richmond, 1980; Spiro *et al*., 1988; Richmond *et al*., 2003; Maruyama *et al*., 2005). In a simplified model, the penetration electric field is eastward in daytime and westward at night, having the same polarity as the quiet time zonal electric field and often a time scale of less than 2 h depending on the magnetospheric conditions present for the shielding electric field to build up (e.g. Kelley *et al*., 1979; Spiro *et al*., 1988; Fejer and Scherliess, 1997; Kelley *et al*., 2003). The disturbance dynamo electric field, on the other hand, has an opposite polarity to the quiet time zonal electric field and often occurs several hours after the storm onset, lasting from several hours to more than a day (Blanc and Richmond, 1980; Scherliess and Fejer 1997; Fuller-Rowell *et al*., 2002). In addition to the electric field effects, the storm-generated equatorward neutral wind also affects the low-latitude ionosphere by changing the field-aligned plasma transport or transporting the plasma from one hemisphere to the other (e.g. Fesen *et al*., 1989; Prölss, 1995; Rishbeth *et al*., 1998; Lin *et al*., 2005b). Disturbances in the neutral composition also a produce positive (increase in plasma density) or negative (decrease in plasma density)

Copyright © The Society of Geomagnetism and Earth, Planetary and Space Sciences (SGEPSS); The Seismological Society of Japan; The Volcanological Society of Japan; The Geodetic Society of Japan; The Japanese Society for Planetary Sciences; TERRAPUB.

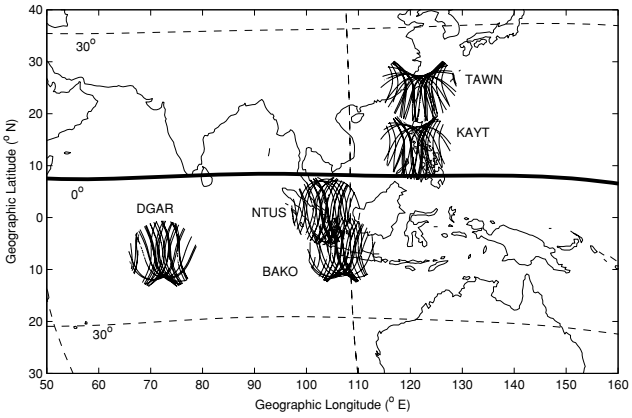

Fig. 1. The sub-ionospheric points of GPS-to-ground receiver links observed by receivers used in this paper. The dashed lines represent the geomagnetic coordinate at the ionospheric height of 300 km obtained by NCAR Apex routine (using the IGRF parameters) (Richmond, 1995) while the bold solid line indicates the geomagnetic equator.

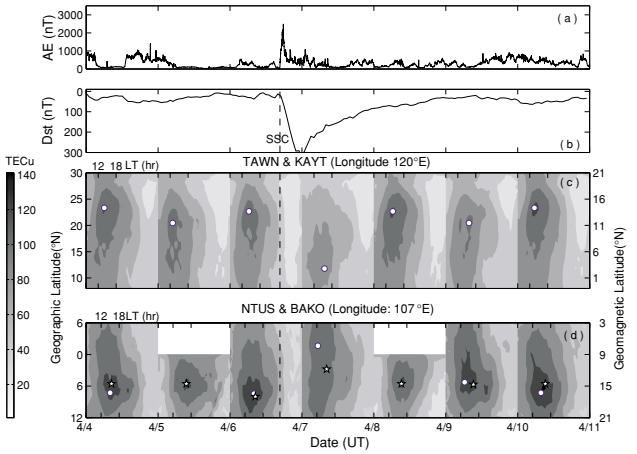

Fig. 2. The AE (a) and Dst indices (b) the LTT map in the northern EIA (c) and equatorial regions and in the southern EIA region (d) during the April 6 storm. The white circles denote the EIA peaks, while the white stars denote the southern EIA peaks obtained from DGAR. The geomagnetic latitude is calculated using the same Apex routine as in Fig. 1.

storm effect through modifying the [O]/[N_2] global distribution that further affects the production and loss of plasma (e.g. Rishbeth *et al*., 1987; Prölss, 1995, 1997; Fuller-Rowell *et al*., 1997; Lu *et al*., 1998; Kil *et al*., 2003; Lin *et al*., 2005a, b).

To study the responses of the low-latitude EIA to the magnetic storm and the importance of the stormtime electric field effects, we used a network of 11 ground-based GPS receivers in the Western Pacific region during the two major magnetic storms on April 6 and July 15, 2000 to observe EIA variations in the two hemispheres simultaneously. Note that both storm events started at the local midnight of the longitude where GPS observations are performed and reached their main phases at the local morning of the same longitudinal sector. The April storm is close to the Equinoctial season while the July storm is close to the solstitial season, which will allow some inter-comparisons between different seasons.

2. Observation results

The approach used here for calculating ionospheric total electron content (TEC) presented here is based on Liu *et al*. (1996) and Tsai and Liu (1999). Figure 1 shows the trajectory of the ionospheric points, which are points on the GPS-to-ground receivers link at ionospheric height (∼300 km), also referred to as sub-ionospheric points, as observed by TAWN (a network of seven stations in Taiwan) and stations called KAYT, BAKO, NTUS, and DGAR. Observations from the TAWN network and KAYT cover the northern EIA and magnetic equator regions, while those from BAKO, NTUS, and DGAR cover the southern EIA region. Figure 2 shows the AE, Dst indices, and observed latitude-time TEC (LTT) map in both the northern and southern EIA regions during the April 4–10, 2000 storm period. Note that the storm sudden commencement (SSC) occurred at 1639 UT on April 6 (vertical dashed line). Figure 2(c) and (d) show the LTT maps observed during April 4–10 (white circles denote the equatorial anomaly crest). It is noted that the receivers (TAWN and KAYT) used for observing the northern EIA and the equatorial regions are located in the 121°E longitude, with a 14° separation between the receivers (BAKO and NTUS) used for observing the southern EIA. Figure 1 reveals that the distortion of the magnetic field in the region is small and that the magnetic latitudes at longitudes 121°E and 107°E are similar. Therefore, the longitudinal effect due to the distortion of the magnetic field is negligible. Due to the lack of data at BAKO and NTUS on April 5 and 8, the TEC derived from DGAR (the southern EIA crests denoted by white star symbol in Fig. 2(d)) is used to fill up the data gap in the southern EIA region for these two days. Although the receiver at DGAR has almost a 40° separation to the BAKO and NTUS longitude, the locations of the EIA crests obtained by DGAR (white stars) show almost same trends in variations as those EIA peaks derived from BAKO and NTUS (white circles) in Fig. 2(d). Thus, the southern EIA observed at DGAR can be a suitable proxy to fill the data gap on April 5 (DOY 096) and 8 (DOY 099). The southern EIA peaks observed by BAKO and NTUS (white circles) appeared earlier in UT than those observed by DGAR (white stars) on April 7, 9, and 10 because the local time of the BAKO and NTUS is about 2–3 h ahead of the DGAR, and storm effects are local time dependent. The most impressive result shown in Fig. 2(c) and (d) is the significant decrease in TEC values in both EIA regions on April 7 while both EIA peak locations move equatorward simultaneously on the same day. The TEC and the EIA peak locations recovered and moved back to their pre-storm conditions on April 8 during the storm recovery phase. Figure 3 shows the observations during the July 12–19, 2000 in the same format as Fig. 2. The SSC occurred at 0942 UT on July 13, 1532 UT on July 14, and 1437 UT on July 15 (vertical dashed lines). According to the Dst values shown in Figs. 2 and 3, the onset time, duration, and the intensity of the April 6 and July 15 storms are very similar. Figure 3(c) and (d) show the LTT maps during July 12–19, 2000. The LTT maps of the southern EIA region are constructed using BAKO data due to the lack of data at NTUS

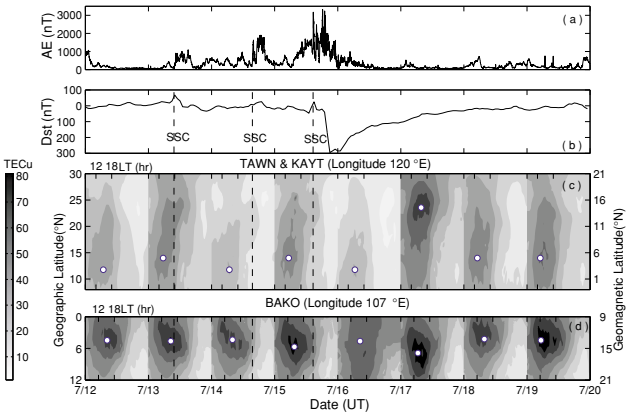

Fig. 3. The AE (a) and Dst indices (b), and the LTT map in the northern EIA and equatorial regions (c) and in the southern EIA region (d) during the July 15 storm. The white circles denote the EIA peaks. The geomagnetic latitude is calculated using the same Apex routine as in Fig. 1.

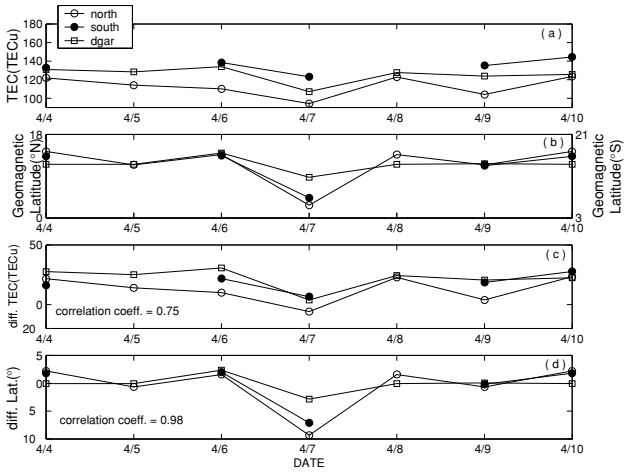

Fig. 4. Day-to-day variations in the TEC values and latitudes of the northern (open circles) and southern (closed circles) EIA peaks extracted from Fig. 2(c) and (d). The square represents the southern EIA peaks observed at DGAR. (a) TEC values, (b) latitudes, (c) TEC values with the monthly quiet day TEC average subtracted, (d) latitudinal locations with the monthly quiet day peak locations subtracted (positive in poleward and negative in equatorward) are shown in both EIA peaks for comparison.

during this period. It can be seen in the northern EIA region that the daytime TEC values have decreased on July 14 and 16 with the equatorward movements of the EIA peaks. In the southern EIA region, TEC values are also lower on July 14 and 16. This decrease in the TEC value in the southern EIA is clearly seen on July 16 with the movement of the southern EIA peak slightly equatorward. Figure 3(c) and (d) also shows strong TEC enhancements and poleward movements of both EIA crests on July 17, indicating that Dst had recovered to its pre-storm value.

To further investigate the EIA variations in the two hemispheres, the EIA peak TEC values and peak locations were extracted from Figs. 2(c) and (d) and 3(c) and (d); these are shown in Figs. 4 (the April storm) and 5 (the July storm), respectively. Figures 4(a) and 5(a) show the day-to-day variations in peaked TEC values in the northern EIA (opened

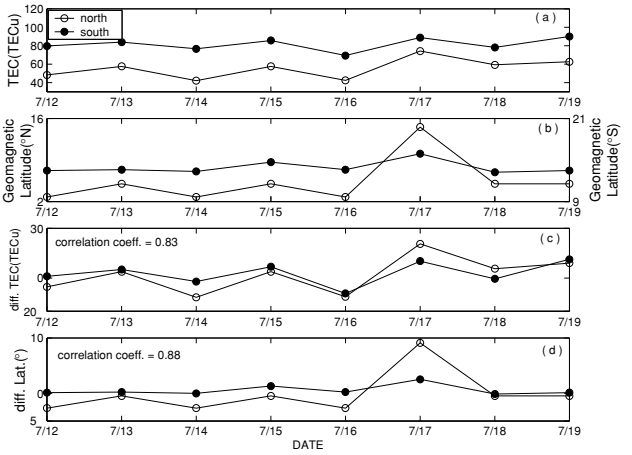

Fig. 5. Day-to-day variations in the TEC values and latitudes of the northern (open circles) and southern (closed circles) EIA peaks extracted from Fig. 3(c) and (d). (a) TEC values, (b) latitudes, (c) TEC values with the monthly quiet day TEC average subtracted, (d) latitudinal locations with the monthly quiet day peak locations subtracted (positive in poleward and negative in equatorward) are shown in both EIA peaks for comparison.

circles) and southern EIA (filled circles) regions; Figs. 4(b) and 5(b) show the day-to-day EIA peak movements in the northern (opened circles with the magnetic latitudes labeled on the left y-axis) and southern (filled circles with the magnetic latitudes labeled on the right y-axis) EIA regions. Figures 4(c) and 5(c) show the day-to-day storm-time variations of peaked TEC, i.e. subtracting the monthly quiet day average of peaked TEC from day-to-day peaked TEC. Figures 4(d) and 5(d) show the storm-time day-to-day EIA peak movements, i.e. subtracting the monthly quiet day average of EIA peak locations from day-to-day EIA peak locations (positive values indicate poleward EIA peak movements while negative values indicate equatorward EIA peak movements). The peaked TEC and peak locations of the southern EIA obtained from DGAR data are also plotted (open squares) in Fig. 4 in order to compare them with the southern EIA peaks obtained from BAKO and NTUS. Note that the monthly quiet day average is obtained by averaging the TEC data with daily summation of Kp indices less than 12+ in the months of April and July. The day-to-day variations of peaked TEC values in the two hemispheres show simultaneous increases or decreases in Fig. 4(c) with a correlation coefficient of 0.75. The EIA peak movements in both hemispheres (Fig. 4(d)) are highly correlated with the correlation coefficient of 0.98. The day-to-day variations of peaked TEC and peak locations in the July event shown in Fig. 5 also reveal high correlations between the northern and southern EIA regions. The day-to-day stormtime peaked TEC in Fig. 5(c) shows a correlation coefficient of 0.83, while the EIA peak movements between the two hemispheres in Fig. 5(d) show a correlation coefficient of 0.88. The most important feature shown in Figs. 4 and 5 is the simultaneous variation in the peaked TEC value and peak locations during the two major storm periods. The EIA peaks become stronger as they move poleward, while the EIA peaks show a weaker intensity as they move equatorward.

3. Discussion

Based on Fig. 2(b), the onset of the April storm onset occurred around 1639 UT on April 6 (0039 LT; April 7, LT=UT+8). Following the main phase of the storm on the next day, April 7, the daytime TEC in both the northern and southern EIA regions shows negative storm effects, with the locations of the EIA peaks having moved significantly equatorward. The possible explanation for the depression of the EIA development on April 7 in Fig. 2 is the suppression of the equatorial plasma fountain due to a weaker eastward electric field. According to the empirical stormtime electric field model at the equatorial region built by Fejer and Scherliess (1995) and the recent theoretical model studied by Fuller-Rowell *et al*. (2002), the storm-generated disturbance neutral winds can reach lower latitudes, producing the disturbance dynamo effects about 4–5 h or even shorter after the storm onset, depending on the amount of the energy deposition to the high latitude region. Thus, a daytime westward perturbation electric field generated by the wind disturbance dynamo process may have been produced to weaken the normal daytime eastward electric field on April 7, more than 10 h after the storm onset, resulting in the suppression of the equatorial plasma fountain and EIA. Figure 3(b) shows that the major July storm started at 1437 UT on July 15 (2237 LT on July 15). The decrease in the TEC in the EIA regions is once again observed the following day, July 16. Both the northern and southern EIA peaks moved equatorward relative to the peak locations on July 15. The decrease in the TEC and the equatorward movements of the EIA crests may again result from the suppression of the EIA development due to the disturbance in the dynamo electric field. Following the suppression of the EIA on July 16, a significant poleward movement of the EIA crests accompanied by an increase in the TEC is observed in both hemispheres on July 17. Simultaneous, strong TEC enhancements and poleward EIA peak movements of the two hemispheres imply that a more enhanced daytime eastward electric field may exist, resulting in a stronger equatorial plasma fountain. Similar TEC enhancement occurred during the recovery phase of the well-known October 29 to November 1, 2003 superstorm (Halloween storm) (Lin *et al*., 2005a). The source of the enhanced daytime eastward electric field is not clear, but it is unlikely to be the eastward penetration electric field, since it is during the later phase of the storm recovery that there are no significant and rapid changes in the AE and Dst indices. The electric field may result from changes in the ionospheric dynamo processes due to changes in the ionospheric conductivities (electron density) by combined storm effects of the direct penetration and disturbance dynamo electric fields or neutral composition perturbation (e.g. Fuller-Rowell *et al*., 1997; Sastri *et al*., 2002; Maruyama *et al*., 2005).

Neutral wind and composition effects are also capable of producing the EIA variations during magnetic storms (e.g. Rishbeth *et al*., 1987; Fesen *et al*., 1989; Prölss 1995; Fuller-Rowell *et al*., 1994, 1996, 1997; Lu *et al*., 1998; Rishbeth *et al*., 1998; Kil *et al*., 2003; Lin *et al*., 2005a, b). The neutral wind and composition effects often result as an asymmetric response of the EIA, especially during solstitial seasons. The asymmetric responses of the northern and southern EIA can be seen in the July storm, with the southern EIA peak showing smaller movement than the northern EIA peak. The asymmetric peak movements in the July event may due to asymmetric background and storm-produced neutral winds (e.g. Fuller-Rowell *et al*., 1996, 1997). For example, on July 16, the stronger summer-to-winter neutral wind suppresses the equatorward movement of the southern EIA peak, while on July 17, the northern peak is closer to the sub-solar point, where the divergence of the wind is more prominent, and the poleward wind may enhance the poleward movement of the northern EIA peak. Since the stormtime neutral winds are highly variable, more observations of the stormtime winds are necessary in interpreting their effect to the EIA variations in detail.

It is worthwhile noting that the composition perturbation—i.e. the decrease of the $[O]/[N_2]$ ratio—may contribute partly to produce the delayed TEC decrease (negative storm effect on the second day of the storm onset). The composition perturbation is formed in the auroral region where the storm-generated energy, mainly the Joule heating, is deposited into the neutral atmosphere where it produces thermal expansion of the neutral air and composition perturbation. The composition perturbation is then carried from high to low latitudes by both background and storm-generated wind fields several hours after the storm (e.g. Rishbeth *et al*., 1987; Prölss, 1987, 1995, 1997; Burns *et al*., 1991, 1995; Fuller-Rowell *et al*., 1994, 1996, 2002; Kil *et al*., 2003; Lin *et al*., 2005a). Asymmetric variations in the north and south hemispheres are clearer in the July event (solstitial season) compared with the April event (Equinoctial season), suggesting that the background neutral winds and compositions contribute to produce asymmetric storm effects. Although both the background and storm-produced neutral wind and composition effects may both contribute to modify the morphology of the EIA, the strong correlations in peaked TEC variations and peak movements of the two hemispheres (Figs. 4 and 5) suggest that the electric field effect may be the major driver in producing the simultaneous EIA variations during the two storm events.

4. Summary

The GPS TEC observations over the EIA regions in the Western Pacific region show that the daytime EIA becomes less-developed approximately 10–12 h after the onset of the storm. The asymmetric response of the EIA in the northern and southern hemispheres shown in the July storm may result from the asymmetric disturbances in neutral wind and composition perturbations due to the asymmetric magnetospheric energy input and background thermosphere conditions. The strong correlations in peaked TEC values and peak latitudes between the northern and southern EIA regions suggest that the disturbance electric field may be the major driver that enhances or weakens the equatorial plasma fountain and the associated EIA morphology.

Acknowledgments. The authors acknowledge the International GNSS Service (IGS), and the Ministry of the Interior of Taiwan for providing ground-based GPS data. This work is partly supported by the National Science Council grant NSC: 95-2111-M-492-001 to the National Space Organization. The National Space Organization is supported by the National Science Council.

References

Anderson, D. N., A theoretical study of the ionospheric F-region equatorial anomaly, I, Theory, *Planet. Space Sci.*, **21**, 409–419, 1973.

Appleton, E. V., Two anomalies in the ionosphere, *Nature*, **157**, 691, 1946.

Balan, N. and G. J. Bailey, Equatorial plasma fountain and its effects: Possibility of an additional layer, *J. Geophys. Res.*, **100**(A11), 21,421–21,432, 1995.

Blanc, M. and A. D. Richmond, The ionospheric disturbance dynamo, *J. Geophys. Res.*, **85**, 1669–1686, 1980.

Buonsanto, Ionospheric Storms—A Review, *Space Sci. Rev.*, **88**, 563–601, 1999.

Burns, A. G., T. L. Killen, and R. G. Roble, A theoretical study of thermospheric composition perturbations during an impulsive geomagnetic storm, *J. Geophys. Res.*, **96**, 14153–14167, 1991.

Burns, A. G., T. L. Killeen, G. R. Carignan, and R. G. Roble, Large enhancements in the O/N_2 ratio in the evening sector of the winter hemisphere during geomagnetic storms, *J. Geophys. Res.*, **100**(A8), 14,661–14,672, 1995.

Duncan, R. A., The equatorial F region of the ionosphere, *J. Atmos. Terr. Phys.*, **18**, 89, 1960.

Fejer, B. G. and L. Scherliess, Time dependent response of equatorial ionospheric electric field to magnetospheric disturbance, *Geophys. Res. Lett.*, **22**, 851–854, 1995.

Fejer, B. G. and L. Scherliess, Empirical models of storm time equatorial zonal electric fields, *J. Geophys. Res.*, **102**(A11), 24047–24056, 10.1029/97JA02164, 1997.

Fesen, C. G., G. Growley, and R. G. Roble, Ionospheric Effects at Low Latitudes During the March 22, 1979, Geomagnetic Storm, *J. Geophys. Res.*, **94**(A5), 5405–5417, 1989.

Fuller-Rowell, T. J., M. V. Codrescu, R. J. Moffett, and S. Quegan, Responseof the thermosphere and ionosphere to geomagnetic storms, *J. Geophys. Res.*, **99**, 3893–3914, 1994.

Fuller-Rowell, T. J., M. V. Codrescu, H. Risbeth, R. J. Moffett, and S. Quegan, On the seasonal response of the thermosphere and ionosphere to geomagnetic storms, *J. Geophys. Res.*, **101**(A2), 2343-2354, 1996.

Fuller-Rowell, T. J., M. V. Codrescu, R. G. Roble, and A. D. Richmond, How Does the Thermosphere and Ionosphere React to a Geomagnetic Storm?, in *Magnetic Storms*, edited by B. T. Tsurutani, W. D. Gonzales and Y. Kamide, AGU Monograph, Washington D. C., 1997.

Fuller-Rowell, T. M., G. H. Millward, A. D. Richmond, and M. V. Codrescu, Storm-time changes in the upper atmosphere at low latitudes, *J. Atmos. Sol. Terr. Phys.*, **64**, 1383, 2002.

Hanson, W. B. and R. J. Moffett, Ionization transport effects in the equatorial F region, *J. Geophys. Res.*, **71**, 5559, 1966.

Jaggi, R. K. and R. A. Wolf, Self-consistent calculation of the motion of a sheet of ions in the magnetosphere, *J. Geophys. Res.*, **78**, 2852–2866, 1973.

Kelley, M. C., B. G. Fejer, and C. A. Gonzales, An explanation for anomalous equatorial ionospheric electric fields associated with a northward turning of the interplanetary magnetic field, *Geophys. Res. Lett.*, **6**, 301–304, 1979.

Kelley, M. C., J. J. Makela, J. L. Chau, and M. J. Nicolls, Penetration of the solar wind electric field into the magnetosphere/ionosphere system, *Geophys. Res. Lett.*, **30**(4), 1158, doi:10.1029/2002GL016321, 2003.

Kil, H., L. J. Paxton, X. Pi, M. R. Hairston, and Y. Zhang, Case study of the 15 July 2000 magnetic storm effects on the ionosphere-driver of the positive ionospheric storm in the winter hemisphere, *J. Geophys. Res.*, **108**(A11), 1391, doi:10.1029/2002JA009782, 2003.

Lin, C. H., A. D. Richmond, J. Y. Liu, H. C. Yeh, L. J. Paxton, G. Lu, H. F. Tsai, and S.-Y. Su, Large-scale variations of the low-latitude ionosphere during the October-November 2003 superstorm: Observational results, *J. Geophys. Res.*, **110**, A09S28, doi:10.1029/2004JA010900, 2005a.

Lin, C. H., A. D. Richmond, R. A. Heelis, G. J. Bailey, G. Lu, J. Y. Liu, H. C. Yeh, and S.-Y. Su, Theoretical study of the low- and midlatitude ionospheric electron density enhancement during the October 2003 superstorm: Relative importance of the neutral wind and the electric field, *J. Geophys. Res.*, **110**, A12312, doi:10.1029/2005JA011304, 2005b.

Liu, J. Y., H. F. Tsai, and T. K. Jung, Total electron content obtained by using the global positioning system, *Terr. Atmos. Oceanic Sci.*, **7**, 107–117, 1996.

Lu, G., X. Pi, A. D. Richmond, and R. G. Roble, Variations of total electron content during geomagnetic disturbances: A model/observation comparison, *Geophys. Res. Lett.*, **25**(3), 253–256, 10.1029/97GL03778, 1998.

Maruyama, N., A. D. Richmond, T. J. Fuller-Rowell, M. V. Codrescu, S. Sazykin, F. R. Toffoletto, R. W. Spiro, and G. H. Millward, Interaction between direct penetration and disturbance dynamo electric fields in the storm-time equatorial ionosphere, *Geophys. Res. Lett.*, **32**, L17105, doi:10.1029/2005GL023763, 2005.

Namba, S. and K.-I. Maeda, *Radio Wave Propagation*, 86 pp., Corona, Tokyo, 1939.

Prölss, G. W., Storm-induced changes in the thermospheric composition at middle latitudes, *Planet. Space Sci.*, **35**, 807–811, 1987.

Prölss, G. W., Ionospheric F-Region Storms, in *Handbook of Atmospheric Electrodynamics*, edited by H. Volland, CRC Press, 1995.

Prölss, G. W., Magnetic storm associated perturbations of the upper atmosphere, in *Magnetic Storms*, Geophys. Monogr. Ser., vol. 98, edited by B. T. Tsurutani *et al.*, pp. 227–241, AGU, Washington D. C., 1997.

Richmond, A. D., Ionospheric electrodynamics using Magnetic Apex Coordinates, *J. Geomag. Geoelectr.*, **47**, 191–212, 1995.

Richmond, A. D., C. Peymirat, and R. G. Roble, Long-lasting disturbances in the equatorial ionospheric electric field simulated with a coupled magnetosphere-ionosphere-thermosphere model, *J. Geophys. Res.*, **108**(A3), 1118, doi:10.1029/2002JA009758, 2003.

Rishbeth, H., How the thermospheric circulation affects the ionospheric F2-layer, *J. Atmos. Sol. Terr. Phys*, **60**, 1385–1402, 1998.

Rishbeth, H., The equatorial F-layer: Progress and puzzles, *Ann. Geophys.*, **18**, 730, 2000.

Rishbeth, H., T. J. Fuller-Rowell, and A. D. Rodger, F-layer storms and thermospheric composition, *Phys. Scripta.*, **36**, 327–336, 1987.

Sastri, J. H., K. Niranjan, and K. S. V. Subbarao, Response of the equatorial ionosphere in the Indian (midnight) sector to the severe magnetic storm of July 15, 2000, *Geophys. Res. Lett.*, **29**(13), 1651, doi:10.1029/2002GL015133, 2002.

Scherliess, L. and B. G. Fejer, Storm time dependence of equatorial disturbance dynamo zonal electric fields, *J. Geophys. Res.*, **102**(A11), 24,037-24,046, 1997.

Senior, C. and M. Blanc, On the control of magnetospheric convection by the spatial distribution of ionospheric conductivities, *J. Geophys. Res.*, **89**, 261–284, 1984.

Spiro, R. W., R. A. Wolf, and B. G. Fejer, Penetration of high-latitude-electric-field effects to low latitudes during SUNDIAL 1984, *Ann. Geophys.*, **6**, 39–50,1988.

Tsai, H. F. and J. Y. Liu, Ionospheric total electron content response to solar eclipses, *J. Geophys. Res.*, **104**, 12657, 1999.

C.-H. Lin (e-mail: clin@nspo.org.tw), J.-Y. Liu, H.-F. Tsai, and C.-Z. Cheng